1.3 kW monolithic linearly polarized single-mode master oscillator power amplifier and strategies for mitigating mode instabilities

Rumao Tao,[1] Pengfei Ma,[1] Xiaolin Wang,[1,*] Pu Zhou,[1,2] and Zejin Liu[1]

[1]*College of Optoelectric Science and Engineering, National University of Defense Technology, Changsha, Hunan 410073, China*
[2]*e-mail: zhoupu203@163.com*
**Corresponding author: chinawxllin@163.com*

Received January 12, 2015; revised March 9, 2015; accepted March 9, 2015; posted March 13, 2015 (Doc. ID 232432); published April 17, 2015

We report on the high-power amplification of a 1064 nm linearly polarized laser in an all-fiber polarization-maintained master oscillator power amplifier, which can operate at an output power level of 1.3 kW. The beam quality (M^2) was measured to be <1.2 at full power operation. The polarization extinction rate of the fiber amplifier was measured to be above 94% before mode instabilities (MIs) set in, which reduced to about 90% after the onset of MI. The power scaling capability of strategies for suppressing MI is analyzed based on a semianalytical model, the theoretical results of which agree with the experimental results. It shows that mitigating MI by coiling the gain fiber is an effective and practical method in standard double-cladding large mode area fiber, and, by tight coiling of the gain fiber to the radius of 5.5 cm, the MI threshold can be increased to three times higher than that without coiling or loose coiling. Experimental studies have been carried out to verify the idea, which has proved that MI was suppressed successfully in the amplifier by proper coiling.

OCIS codes: (060.2320) Fiber optics amplifiers and oscillators; (060.2420) Fibers, polarization-maintaining; (060.2430) Fibers, single-mode.
http://dx.doi.org/10.1364/PRJ.3.000086

1. INTRODUCTION

Many applications, such as coherent lidar systems, nonlinear frequency conversion, and coherent beam combining architectures, require high-power linearly polarized laser sources with near-diffraction-limited beam quality [1–6]. Recently, a linearly polarized fiber laser with 1 kW output power has been achieved in a monolithic fiber Bragg grating (FBG)-based Fabry–Perot cavity [7], which employed a pair of high-power FBGs. It is a technological challenge to design an FBG that can withstand multikilowatt power, and further power scaling may encounter some technological difficulties. Fiber laser systems based on master oscillator power amplifiers (MOPAs) are typically capable of reaching high output powers, while also offering more flexibility in terms of linewidth and polarization control than a simple grating-based laser [8]. Most of the high-power fiber laser systems with random polarized output are based on MOPAs at the moment, which has achieved output power as high as tens of kilowatts. However, power scaling of linearly polarized MOPAs to multikilowatt level is currently limited by the onset of mode instabilities (MIs) [8–10]. Although lots of work has been carried out to deal with MI experimentally and theoretically [11–27], few methods to mitigate MI effectively in the all-fiber MOPA configuration with standard step-index large mode area (LMA) fiber have been proposed, and MI-free power scaling in an all-fiber MOPA, which is based on standard step-index polarization-maintaining (PM) LMA fibers, is even more challenging.

In this paper, we present a 1.3-kW-level all-fiber Yb-doped PM fiber amplifier with linearly polarized operation and near-diffraction-limited beam quality. We also discuss experiments, coupled with numerical modeling, to estimate the further power scaling capability of various strategies to mitigate MI. Numerical modeling results suggest that MI-free single-mode output powers in excess of 3 kW could be realized in standard step-index LMA fiber.

2. EXPERIMENTAL SETUP AND RESULTS

A monolithic, all-fiber, Yb-doped PM fiber amplifier is shown in Fig. 1. The seed laser in the experiment is a 50 mW linearly polarized continuous-wave laser with central wavelength at ~1064 nm, which was then amplified in two preamplifier stages to ~25 W. The main amplifier consists of a 20 m PM double-clad LMA Yb-doped fiber (YDF) with 21 μm diameter/0.064 NA core and 400 μm diameter/0.44 NA cladding, which is coiled in a radius of 10 cm. Six multimode fiber-pigtailed 915 nm laser diodes were used to pump the gain fiber through a $(6+1)\times 1$ signal/pump combiner, which can provide a maximum pump power of about 2 kW. An approximately 0.75 m long passive fiber is spliced to the gain fiber for power delivery, the output end of which is angle cleaved in order to prevent parasitic feedback from Fresnel reflection.

The achieved output power at different pump power levels is shown in Fig. 2(a), which is measured after the output beam passed through a dichroic mirror. The slope efficiency of the amplifier is 65.3% with respect to launched pump power, and the pump-limited maximum output power is 1261 W. The inset in Fig. 2(a) shows the measured far-field beam profile at the maximal operation power, and the beam quality factor M^2 is

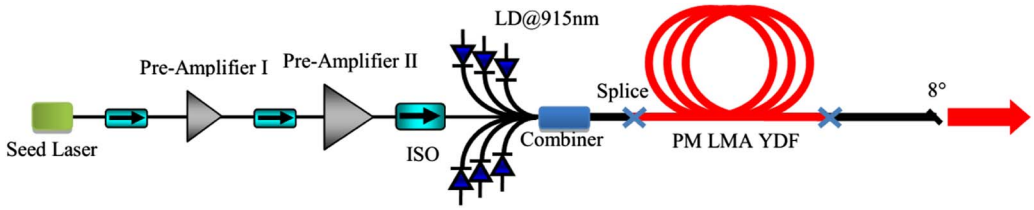

Fig. 1. Architecture of the all-fiber PM amplifier.

measured by M^2-200 s (Spiricon) to be <1.2 in both directions. Figure 2(b) shows the measured spectra (by an optical spectrum analyzer, AQ6370C Yokogawa) at full power operation, which shows that a high signal-to-noise ratio (SNR) has been achieved and shows no signs of parasitic lasing or significant levels of amplified spontaneous emission. Figure 2(c) shows the measurement of the polarization extinction rate (PER) for different pump power levels. It can be seen that the PER is above 90% in the whole range, which indicates a linearly polarized operation. The sudden degradation from 94% to 90% above 1.2 kW was caused by MI, while the slow degradation of PER as lasing power increases may be caused by the temperature increase of the fiber.

An InGaAs photodetector (150 MHz, 700–1800 nm, Thorlabs) with a pinhole of 1.5 mm diameter was put in the center of the collimated beam to monitor the onset of MI [14,15,25]. Time traces at different output powers are shown in Fig. 3(a), and the DC component of the electrical signal is removed. From Fig. 3(a), we can obtain that although the output power is still pump limited to 1.26 kW, we are operating at the MI threshold (@1.26 kW). Although the MI has set in, deterioration of beam quality has not been observed [Fig. 2(a)], which is due to the fact that the fraction of high-order mode (HOM) is relatively small at the beginning of MI [24]. It also shows that, at the onset of MI, the amplitude of the time trace is close to the same as that without MI in the time period T1 and becomes higher than that without MI in time period T2. Applying Fourier analysis on the time traces to calculate the corresponding Fourier spectra, we obtained the frequency distribution of the beam fluctuation as shown in Fig. 3(b). The frequency components of the beam fluctuations distributed in the range of 0–200 Hz at power of 1.14 kW, which means

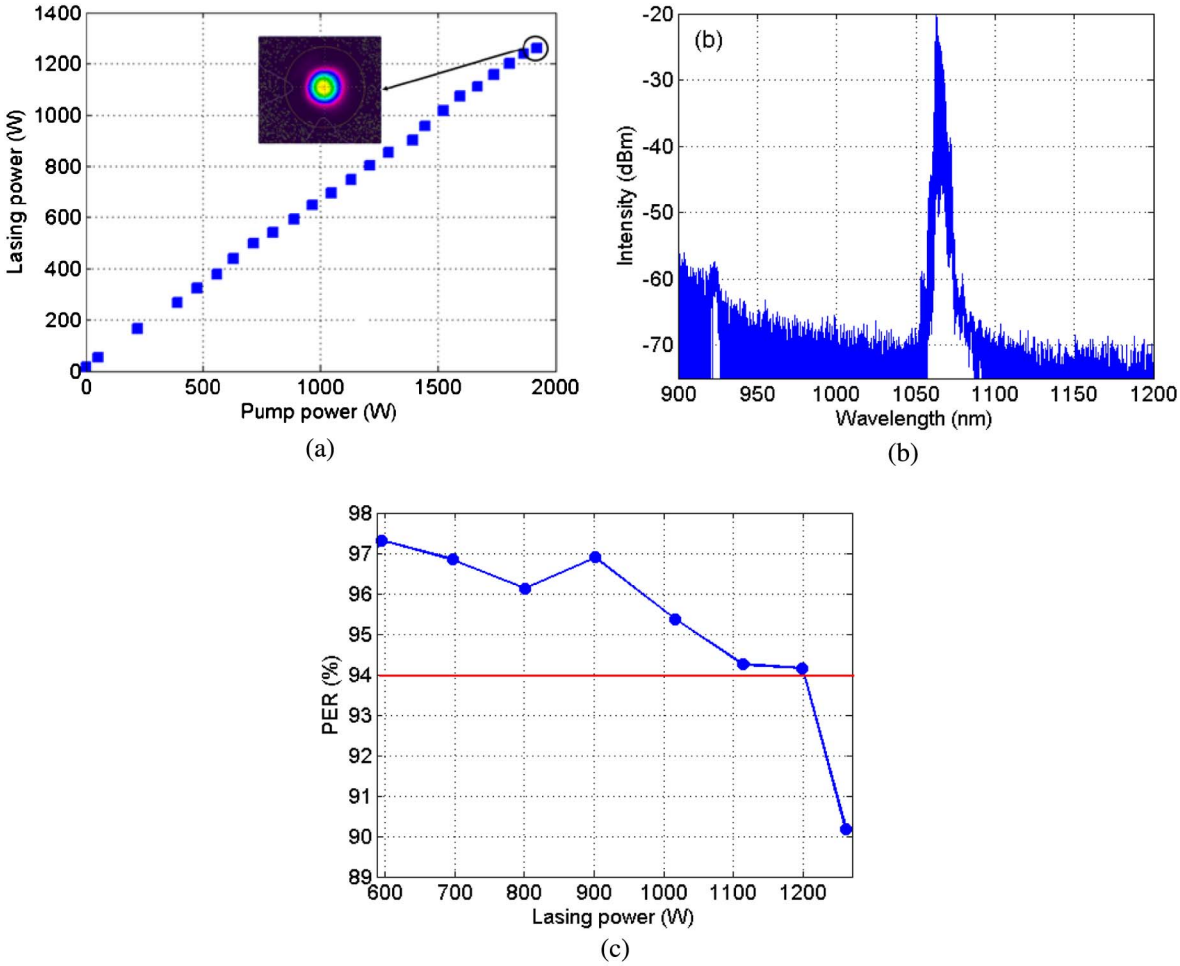

Fig. 2. Output characteristics of the main amplifier. (a) Output power. (b) Output spectrums. (c) PER.

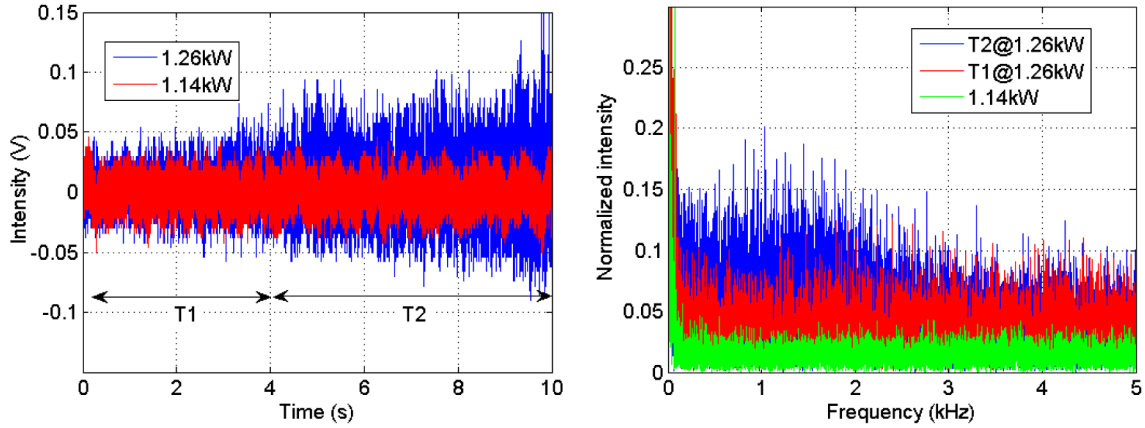

Fig. 3. Fluctuation characteristics of the output beam. (a) Time traces. (b) Frequency distribution.

that the output beam profile is stable; however, further increasing the output power, frequency components in 0–3 kHz showed up as well as background noise increased, which indicated that the sign of the instable beam profile appeared and that the amplifiers were approaching the threshold. Similar to the observation in [26], the instability of MI has a grown process: at the start (T1), only background noise increases, which means a stable beam profile and indicates that MI may relate to noise [17]; after a few seconds (T2), frequency components show up, which indicates an unstable beam profile. After multiple power cycles near the maximum power, we observed that the threshold reduced to below 1.2 kW and was finally stabilized around 1180 W, which may due to the fiber degradation [9,27]. It is claimed in [27] that the fiber degradation, which results in the decrease of MI threshold power, is related to the color center formation commonly associated with photodarkening phenomena. The fiber degradation—photodarkening—that induces the threshold decrease of MI is hard to quantify directly: although the MI threshold power reduced, the measured output lasing power remained the same, which means that the system can be considered nearly "photodarkening free" from the practical application. This is due to the fact that the gain available in the fiber will compensate for the extra losses introduced by photodarkening [28]. Based on the aforementioned discussion, it is hard to quantify the fiber degradation directly [29]. However, the MI threshold decreasing can be considered as an indication of the degradation indirectly. If we take it as the criterion to quantify the fiber degradation, the fiber used in the experiment is degraded by 6% $((P_{\text{initial}} - P_{\text{final}})/P_{\text{initial}})$.

3. STRATEGIES FOR SUPPRESSING MODE INSTABILITIES

A. Theoretical Model

As shown in the previous section, the linearly polarized single-mode output of the fiber laser is limited by the onset of MI. Work should be carried out to study the further power scaling of the amplifier with single-mode linearly polarized output. One way is to carry out numerical study on MI and to find a way to mitigate this phenomenon effectively. In high-power fiber laser systems, most of the fibers are weakly guided fibers, where optical fields can be well approximated by linearly polarized (LP) modes. For linearly polarized fiber lasers, the optical field of the signal propagating in the fiber is expressed in the conventional LP mode representations

$$E(r,\phi,z,t) = \sum_{m=0}^{\infty}\sum_{l=1}^{\infty} A_{ml}(z,t)\psi_{ml}(r,\phi)e^{j(\beta_{ml}z-\omega_{ml}t)} + \text{c.c.}, \quad (1)$$

where m and l are the azimuthal and radial mode numbers, respectively. $A_{ml}(z,t)$, β_{ml}, and $\psi_{ml}(r,\phi)$ are the slowly varying mode amplitudes, propagation constants, and normalized mode profiles of the LP_{ml} mode. Assuming the case in which the fiber amplifiers are operating below or near the MI threshold, we therefore include only the fundamental mode (LP_{01}) and one of the two degenerate LP_{11} modes, and the subscripts of 01 and 11 are replaced with 1 and 2 for the LP_{01} mode and the LP_{11} mode, respectively. Then the signal intensity I_s can be written as

$$I_s(r,\phi,z,t) = 2n_0\varepsilon_0 cE(r,\phi,z,t)E(r,\phi,z,t)^* = I_0 + \tilde{I} \quad (2)$$

with

$$I_0 = I_{11}(z,t)\psi_1(r,\phi)\psi_1(r,\phi) + I_{22}(z,t)\psi_2(r,\phi)\psi_2(r,\phi), \quad (3a)$$

$$\tilde{I} = I_{12}(z,t)\psi_1(r,\phi)\psi_2(r,\phi)e^{j(qz-\Omega t)} + I_{21}(z,t)\psi_1(r,\phi)\psi_2(r,\phi)e^{-j(qz-\Omega t)}, \quad (3b)$$

$$I_{kl}(z,t) = 4n_0\varepsilon_0 cA_k(z,t)A_l^*(z,t), \quad (3c)$$

$$q = \beta_1 - \beta_2, \quad \Omega = \omega_1 - \omega_2. \quad (3d)$$

Here n_0 is the refractive index of the fiber core.

The temperature distribution is governed by the heat transportation equation, which is given by

$$\nabla^2 T(r,\phi,z,t) + \frac{Q(r,\phi,z,t)}{\kappa} = \frac{1}{\alpha}\frac{\partial T(r,\phi,z,t)}{\partial t}, \quad (4)$$

where $\alpha = \kappa/\rho C$, ρ is the density, C is the specific heat capacity, and κ is the thermal conductivity. Since the heat in high-power fiber amplifiers is mainly generated from the quantum

defect and absorption, the volume heat-generation density Q can be approximately expressed as

$$Q(r,\phi,z,t) \cong g(r,\phi,z,t)\left(\frac{v_p - v_s}{v_s}\right) I_s(r,\phi,z,t), \tag{5a}$$

and $g(r,\phi,z,t)$ is the gain of the amplifier

$$g(r,\phi,z,t) = [(\sigma_s^a + \sigma_s^e)n_u(r,\phi,z,t) - \sigma_s^a]N_{\mathrm{Yb}}(r,\phi), \tag{5b}$$

where $v_{p(s)}$ represents the optical frequencies, σ_s^a and σ_s^e are the signal absorption and emission cross sections, σ_p^a and σ_p^e are the pump absorption and emission cross sections, $N_{\mathrm{Yb}}(r,\phi)$ is the doping profile, and the steady-state population inversion n_μ is given in [16]. For the case in which the fiber is doped uniformly, $N_{\mathrm{Yb}}(r,\phi)$ is a constant across the doping area, which is equal to the dopant concentration N_0.

Assume that the fiber is water cooled; the appropriate boundary condition for the heat equation at the fiber surface is

$$\kappa\frac{\partial T}{\partial r} + h_q T = 0, \tag{6}$$

where h_q is the convection coefficient for the cooling fluid. By adopting the integral-transform technique to separate variables in the cylindrical system [30], Eq. (4), combined with Eqs. (5) and (6), can be solved as

$$T(r,\phi,z,t) = \frac{1}{\pi}\frac{\alpha\sigma}{\eta}\sum_v \sum_{m=1}^{\infty}\frac{J_v(\delta_m r)}{H(\delta_m)}\int_{t'=0}^{t}\begin{bmatrix} B_{11}(\phi,z)I_{11}(z,t') + B_{22}(\phi,z)I_{22}(z,t') \\ +B_{12}(\phi,z)I_{12}(z,t')e^{j(qz-\Omega t')} + B_{12}(\phi,z)I_{12}^*(z,t')e^{-j(qz-\Omega t')}\end{bmatrix} e^{-\alpha\delta_m^2(t-t')}\mathrm{d}t' \tag{7}$$

with

$$B_{kl}(\phi,z) = \begin{cases} \int_0^{2\pi}\mathrm{d}\phi'\int_0^R g_0 J_v(\delta_m,r')\cos v(\phi-\phi')\dfrac{\psi_k(r',\phi')\psi_k(r',\phi')}{1+I_0/I_{\mathrm{saturation}}}\mathrm{d}r', & k=l \\ \int_0^{2\pi}\mathrm{d}\phi'\int_0^R g_0 J_v(\delta_m,r')\cos v(\phi-\phi')\dfrac{\psi_k(r',\phi')\psi_l(r',\phi')}{(1+I_0/I_{\mathrm{saturation}})^2}\mathrm{d}r', & k\neq l \end{cases}, \tag{8a}$$

$$H(\delta_m) = \int_0^R r J_v^2(\delta_m,r)\mathrm{d}r, \qquad \sigma = \frac{\eta}{\kappa}\left(\frac{v_p - v_s}{v_s}\right), \tag{8b}$$

where $v = 0, 1, 2, 3\ldots$ and we replace π by 2π for $v = 0$, η is the thermal-optic coefficient, R is the radius of the inner cladding, g_0 is the small signal gain, and $I_{\mathrm{saturation}}$ is the saturation intensity. $J_v(\cdot)$ is a Bessel function of the first kind, and δ_m represents the positive roots of $\delta_m J_v'(\delta_m R) + \frac{h_q}{\kappa}J_v(\delta_m R) = 0$. Solving the time-dependent temperature equation by the integral-transform technique is different from other models, such as solving the temperature equation using different summations of Bessel functions [18] or Green's functions [17,19,20], or other numerical methods [13]. Considering the effective refractive index of gain from the amplifier, the total refractive index, which attributes to gain ($n_g \le n_0$) and nonlinearity ($n_{\mathrm{NL}} \le n_0$), can be expressed as

$$n^2 = (n_0 + n_g + n_{\mathrm{NL}})^2 \cong n_0^2 - j\frac{g(r,\phi,z,t)n_0}{k_0} + 2n_0 n_{\mathrm{NL}}, \tag{9}$$

where n_{NL} is given by

$$\begin{aligned} n_{\mathrm{NL}}(r,\phi,z,t) &= \eta T(r,\phi,z,t) \\ &= h_{11}(r,\phi,z,t) + h_{22}(r,\phi,z,t) \\ &\quad + h_{12}(r,\phi,z,t)e^{jqz} + h_{21}(r,\phi,z,t)e^{-jqz} \end{aligned} \tag{10}$$

with

$$h_{kl}(r,\phi,z,t) = \begin{cases} \frac{\alpha\sigma}{\pi}\sum_v\sum_{m=1}^{\infty}\frac{J_v(\delta_m r)}{H(\delta_m)}\int_0^t B_{kk}(\phi,z)I_{kk}(z,t')e^{-\alpha\delta_m^2(t-t')}\mathrm{d}t', & k=l \\ \frac{\alpha\sigma}{\pi}\sum_v\sum_{m=1}^{\infty}\frac{J_v(\delta_m r)}{H(\delta_m)}\int_0^t B_{kl}(\phi,z)I_{kl}(z,t')e^{-\alpha\delta_m^2(t-t')-j\Omega t'}\mathrm{d}t', & k\neq l \end{cases}. \tag{11}$$

Inserting Eqs. (1) and (10) into the wave equation, after very tedious but straightforward derivations, we have obtained the coupled-mode equations

$$\frac{\partial|A_1|^2}{\partial z} = \iint g(r,\phi,z)\psi_1\psi_1 r\mathrm{d}r\mathrm{d}\phi|A_1|^2, \tag{12a}$$

$$\frac{\partial|A_2|^2}{\partial z} = \left[\iint g(r,\phi,z)\psi_2\psi_2 r\mathrm{d}r\mathrm{d}\phi + |A_1|^2\chi(\Omega,t)\right]|A_2|^2 \tag{12b}$$

with

$$\chi(\Omega) = 2\frac{n_0\omega_2^2}{c^2\beta_2}\,\mathrm{Im}\left(\iint \bar{h}_{12}\psi_1\psi_2 r\mathrm{d}r\mathrm{d}\phi\right), \tag{13a}$$

$$\bar{h}_{kl}(r,\phi,z) = \frac{\alpha\sigma}{\pi}\sum_v\sum_{m=1}^{\infty}\frac{J_v(\delta_m r)}{H(\delta_m)}\frac{B_{kl}(\phi,z)}{\alpha\delta_m^2 - j\Omega}. \tag{13b}$$

By taking the similar derivation process in [17], we can obtain the HOM content for the quantum noise (QN) induced MI from Eq. (1), which is given as

$$\xi(L) \approx \frac{\hbar\omega_0}{P_1(L)}\sqrt{\frac{2\pi}{\int_0^L P_1(z)|\chi''(\Omega_0)|\mathrm{d}z}} \times \exp\left\{\int_0^L\left[\iint g(r,\phi,z)\psi_2\psi_2 r\mathrm{d}r\mathrm{d}\phi\right]\mathrm{d}z + \int_0^L P_1(z)\chi(\Omega_0)\mathrm{d}z\right\}, \quad (14)$$

where L is the length of the gain fiber. For the other case in which MI is seeded by intensity noise, we can obtain

$$\begin{aligned}\xi(L) &\approx \xi_0 \exp\left[\int_0^L \mathrm{d}z \iint g(r,\phi,z)(\psi_2\psi_2-\psi_1\psi_1)r\mathrm{d}r\mathrm{d}\phi - \alpha_{\mathrm{coil}}L_{\mathrm{coil}}\right] \\ &+ \frac{\xi_0}{4}\sqrt{\frac{2\pi}{\int_0^L P_1(z)|\chi''(\Omega_0)|\mathrm{d}z}}R_N(\Omega_0) \\ &\times \exp\left[\int_0^L \mathrm{d}z \iint g(r,\phi,z)(\psi_2\psi_2-\psi_1\psi_1)r\mathrm{d}r\mathrm{d}\phi \right. \\ &\left. + \int_0^L P_1(z)\chi(\Omega_0)\mathrm{d}z - \alpha_{\mathrm{coil}}L_{\mathrm{coil}}\right], \quad (15)\end{aligned}$$

where $R_N(\Omega)$ is the relative intensity noise (RIN) of the input signal, ξ_0 is the initial HOM content, α_{coil} is the bend-induced power loss by fiber coiling, and L_{coil} is the length of the coiled length. Here bend-induced loss is taken into consideration in a simple way, and the effect of bend-induced mode distortion has not been considered. Here we achieved a semianalytical model, which is different from the numerical model in [31]. In [31], the integral-transform technique was also employed to solve the time-dependent temperature equation.

B. Numerical Results

In this section, we have calculated the MI threshold power of the amplifier based on the model. The parameters of the fiber are the same as those in the experiment, which are listed in Table 1. The fiber was doped uniformly, and $N_{\mathrm{Yb}}(r,\phi) = N_0$. The initial signal power is 20 W.

First, we calculated the MI threshold power of the amplifier. Figure 4(a) shows the HOM content versus the pump power. It is shown that the quantum-induced-MI threshold power is about 4.7 kW. However, the intensity noise of the signal (RIN $= 10^{-10}$, which corresponds to a laser with high RIN, which yields a realistic MI threshold [32,33]) reduces the threshold to about 2 kW, which agrees well with the experimental results. The initial HOM is set to be 0.01. By reducing the intensity noise of the signal (RIN $= 10^{-11}$), the MI threshold power can be increased by ~300 W, which means that measures taken to reduce the intensity noise of the input signal result in only modest improvements in the MI threshold and adding to the overall complexity of the system [34]. The influence of HOM power was also calculated in Fig. 4(b), which shows that the efforts to optimize the in-coupling of the signal have little impact on the MI threshold, which agrees with the experimental results [13].

It is reported in [35] that the MI threshold power can be increased obviously by increasing cladding diameters. This is contradictive to those reported in [11], which shows that the improvement by increasing the cladding diameter was not large enough for significant power scaling. To study the effect of cladding diameter on MI threshold power, we calculated the MI threshold pump power for different cladding diameters, which is shown in Fig. 5. The computed thresholds are seen to rise with increasing cladding diameters and the resulting increasing degree of population saturation [35]. However, for fiber with larger core diameters, the improvement becomes less

Table 1. Parameters of Test Amplifier

R_{core}	10.5 μm
R	200 μm
n_0	1.45146
NA	0.064
λ_p	915 nm
λ_s	1064 nm
h_q	5000 W/(m^2 K)
η	1.2×10^{-5} K^{-1}
κ	1.38 W/(Km)
ρC	1.54×10^{6} J/(Km^3)
σ_p^a	6.04×10^{-25} m^2
σ_p^e	1.96×10^{-26} m^2
σ_s^a	6.0×10^{-27} m^2
σ_s^e	3.58×10^{-25} m^2
N_0	3.5×10^{25} m^{-3}

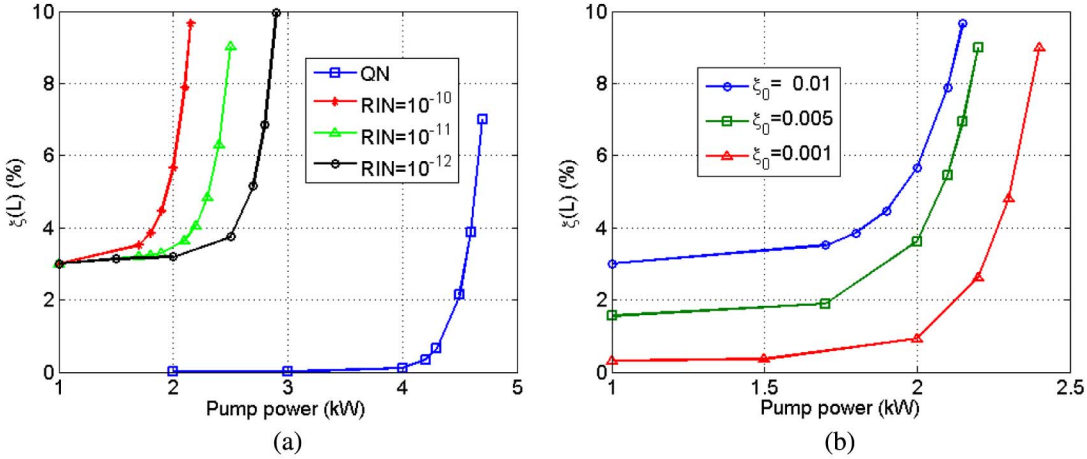

Fig. 4. Threshold calculation of the fiber amplifier.

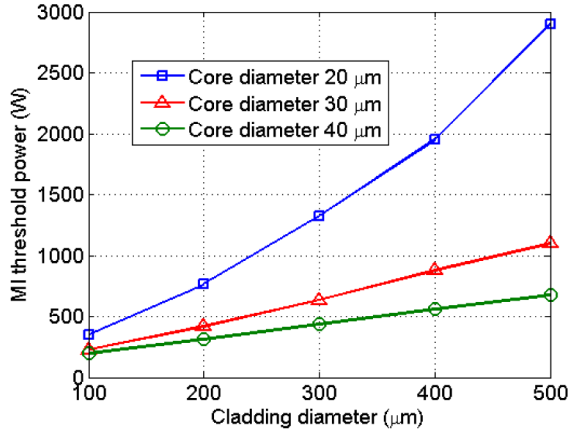

Fig. 5. Threshold pump power for different fiber cladding diameters.

significant, which explained the experimental results in [11]. Although MI threshold power can be improved by increasing cladding diameter, longer length is required for fibers with larger cladding diameter to maintain good amplifier efficiency, which makes other nonlinear effect suppression more challenging.

Coiling the fiber with a diameter small enough to induce mode-dependent bend losses can suppress HOM effectively [36], which can improve the MI threshold [23,37]. The threshold power of the amplifier with tight coiling was calculated in Fig. 6. Bend losses for the LP_{11} mode are calculated using the method of Marcuse [38]: the bending loss is 2.4 dB/m for bending radius of 6.5 cm, 6 dB/m for 6 cm, and 14 dB/m for 5.5 cm. An additional correction factor, yielding an effective bending diameter, incorporates the material stress-optic effect [39]. In practice, only the first half of the gain fiber is coiled with small diameter, so L_{coil} is set to be 6 m. These coiling radii are chosen for long-term use. This shows that tight coiling of the fiber can increase the MI threshold power significantly: when coiling at the radius of 5.5 cm, the MI threshold is three times higher than that without coiling or loose coiling, which means that tight coiling of the gain fiber is an effective method to mitigate MI in the all-fiber MOPA configuration with standard step-index LMA fiber. For the case in the experiment, MI is no longer a limitation since the onset of

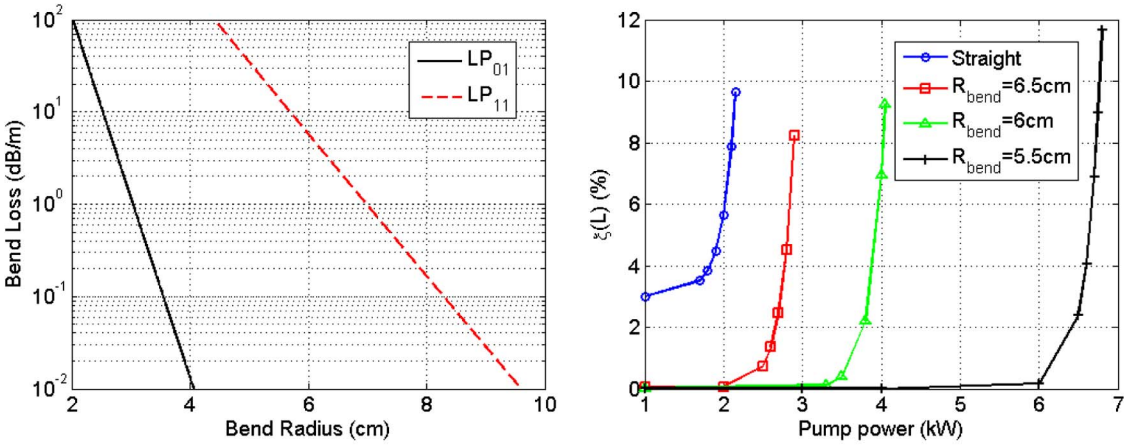

Fig. 6. Effect of coiling on MI threshold power.

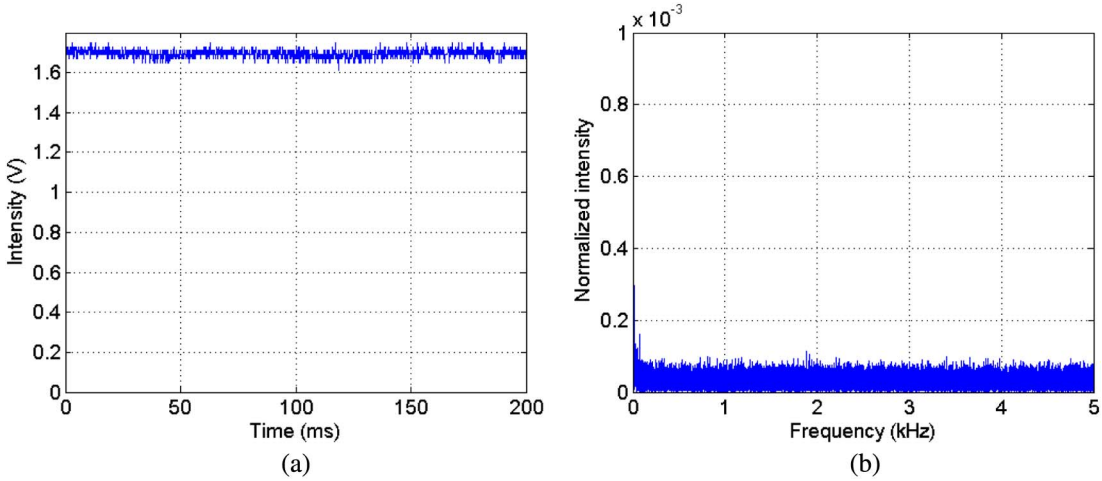

Fig. 7. Fluctuation characteristics of the output beam after tight coiling. (a) Time trace (b) Frequency distribution.

other nonlinear effects, such as SBS and/or SRS, should come into consideration first.

C. Experimental Validation

To verify our theoretical predication of the effect of coiling, we have rebuilt our fiber amplifiers with gain fiber coiled at the diameter of ~12 cm. Then we have an MI-free 1280 W linearly polarized single-mode laser, and all phenomena related to the onset of MI, such as temporal fluctuation and PER degradation, have vanished [as shown in Figs. 7(a) and 7(b)]. Due to the available pump power, the power scaling capabilities by the coiling method have not been fully exploited. The advantage of employing the coiling technique is that it is straightforward to implement, as most fibers are coiled in packaging anyway, and no special gain profiles are necessary to give preferential gain to fiber modes. In addition, the PER of the amplifier has also been improved to ~96% at the maximal operation. The results also indicate that MI can be mitigated by designing fiber with an improved delocalization of HOM, such as chirally coupled core (CCC) fiber [40], leakage channel fibers [41], and all-solid photonic bandgap fibers [42].

4. CONCLUSIONS

We have generated a high-power linearly polarized single-mode output laser from a Yb-doped PM fiber amplifier, which operated at ~1064 nm. The slope efficiency of the amplifier is 65.3% with respect to launched pump power, and the maximal output power is 1261 W. The M2 at full power operation is measured to be <1.2 in both directions. The linear polarization operation was deteriorated by the onset of MI above 1.2 kW. The PER is measured to be >94% without MI, which reduced to about 90% after the onset of MI. A novel theoretical model to study MI has been built up, and the numerical results agree well with the experimental observation. Various methods to improve the power scaling capability of the amplifier without MI have been studied numerically, which reveal that MI can be suppressed by proper coiling and the amplifier in the paper has the potential to deliver MI-free 3 kW output power. An additional experiment has been carried out to study the effect of coiling on MI, which rebuilt the amplifier with tighter coiling. It is shown that MI was suppressed successfully in the amplifier by tight coiling.

ACKNOWLEDGMENTS

The authors acknowledge the support of Hanwei Zhang, Xiong Wang, Hailong Yu, and Baolai Yang. The research leading to these results has received funding from the program for the National Science Foundation of China under Grant No. 61322505, the program for New Century Excellent Talents in University, the Innovation Foundation for Excellent Graduates in National University of Defense Technology under Grant No. B120704, and the Hunan Provincial Innovation Foundation for Postgraduate under Grant No. CX2012B035.

REFERENCES

1. C. B. Olausson, A. Shirakawa, M. Chen, J. K. Lyngsø, J. Broeng, K. P. Hansen, A. Bjarklev, and K. Ueda, "167 W, power scalable ytterbium-doped photonic bandgap fiber amplifier at 1178 nm," Opt. Express **18**, 16345–16352 (2010).
2. J. Wang, J. Hu, L. Zhang, X. Gu, J. Chen, and Y. Feng, "A 100 W all-fiber linearly-polarized Yb-doped single-mode fiber laser at 1120 nm," Opt. Express **20**, 28373–28378 (2012).
3. S. Mo, S. Xu, X. Huang, W. Zhang, Z. Feng, D. Chen, T. Yang, and Z. Yang, "A 1014 nm linearly polarized low noise narrow linewidth single-frequency fiber laser," Opt. Express **21**, 12419–12423 (2013).
4. J. Liu, H. Shi, K. Liu, Y. Hou, and P. Wang, "210 W single-frequency, single-polarization, thulium-doped all-fiber MOPA," Opt. Express **22**, 13572–13578 (2014).
5. B. Samson and A. Carter, "Recent progress on power scaling narrow linewidth fiber amplifiers and their applications," Rev. Laser Eng. **41**, 714–717 (2010).
6. A. Carter, J. Edgecumbe, D. P. Machewirth, J. Galipeau, B. Samson, K. Tankala, and M. O'Connor, "Recent progress in the development of kW-level monolithic PM-LMA fiber amplifiers," Proc. SPIE **6344**, 6344F (2006).
7. S. Belke, F. Becker, B. Neumann, S. Ruppik, and U. Hefter, "Completely monolithic linearly polarized high-power fiber laser oscillator," Proc. SPIE **8961**, 896124 (2014).
8. B. Samson, A. Carter, and K. Tankala, "Rare-earth fibres power up," Nat. Photonics **5**, 466–467 (2011).
9. K. Brar, M. Savage-Leuchs, J. Henrie, S. Courtney, C. Dilley, R. Afzal, and E. Honea, "Threshold power and fiber degradation induced modal instabilities in high power fiber amplifiers based on large mode area fibers," Proc. SPIE **8961**, 89611R (2014).
10. C. Wirth, T. Schreiber, M. Rekas, I. Tsybin, T. Peschel, R. Eberhardt, and A. Tünnermann, "High-power linear-polarized narrow linewidth photonic crystal fiber amplifier," Proc. SPIE **7580**, 75801H (2010).
11. C. Robin, I. Dajani, C. Zeringue, B. Ward, and A. Lanari, "Gain-tailored SBS suppressing photonic crystal fibers for high power applications," Proc. SPIE **8237**, 82371D (2012).
12. M. Karow, H. Tunnermann, J. Neumann, D. Kracht, and P. Wessels, "Beam quality degradation of a single frequency Yb-doped photonic crystal fiber amplifier with low mode instability threshold power," Opt. Lett. **37**, 4242–4244 (2012).
13. B. Ward, C. Robin, and I. Dajani, "Origin of thermal modal instabilities in large mode area fiber amplifiers," Opt. Express **20**, 11407–11422 (2012).
14. N. Haarlammert, O. de Vries, A. Liem, A. Kliner, T. Peschel, T. Schreiber, R. Eberhardt, and A. Tünnermann, "Build up and decay of mode instability in a high power fiber amplifier," Opt. Express **20**, 13274–13283 (2012).
15. R. Tao, P. Ma, X. Wang, P. Zhou, and Z. Liu, "Experimental study on mode instabilities in all-fiberized high-power fiber amplifiers," Chin. Opt. Lett. **12**, 020603 (2014).
16. A. Smith and J. Smith, "Mode instability in high power fiber amplifiers," Opt. Express **19**, 10180–10192 (2011).
17. K. R. Hansen, T. T. Alkeskjold, J. Broeng, and J. Lægsgaard, "Theoretical analysis of mode instability in high power fiber amplifiers," Opt. Express **21**, 1944–1971 (2013).
18. L. Dong, "Stimulated thermal Rayleigh scattering in optical fibers," Opt. Express **21**, 2642–2656 (2013).
19. A. V. Smith and J. J. Smith, "Steady-periodic method for modeling mode instability in fiber amplifiers," Opt. Express **21**, 2606–2623 (2013).
20. K. R. Hansen, T. T. Alkeskjold, and J. Lægsgaard, "Impact of gain saturation on the mode instability threshold in high-power fiber amplifiers," Opt. Express **22**, 11267–11278 (2014).
21. W.-W. Ke, X.-J. Wang, X.-F. Bao, and X.-J. Shu, "Thermally induced mode distortion and its limit to power scaling of fiber lasers," Opt. Express **21**, 14272–14281 (2013).
22. C. Jauregui, H. Otto, F. Stutzki, F. Jansen, J. Limpert, and A. Tünnermann, "Passive mitigation strategies for mode instabilities in high-power fiber laser systems," Opt. Express **21**, 19375–19386 (2013).
23. A. V. Smith and J. J. Smith, "Maximizing the mode instability threshold of a fiber amplifier," arXiv:1301.3489 (2013).
24. H.-J. Otto, C. Jauregui, F. Stutzki, F. Jansen, J. Limpert, and A. Tünnermann, "Controlling mode instabilities by dynamic mode excitation with an acousto-optic deflector," Opt. Express **21**, 17285–17298 (2013).
25. H.-J. Otto, F. Stutzki, F. Jansen, T. Eidam, C. Jauregui, J. Limpert, and A. Tünnermann, "Temporal dynamics of mode instabilities in high-power fiber lasers and amplifiers," Opt. Express **20**, 15710–15722 (2012).
26. R. Tao, P. Ma, X. Wang, P. Zhou, and Z. Liu, "Study of mode instabilities in high power fiber amplifiers by detecting scattering light,"

presented at International Photonics and OptoElectronics Meetings, Wuhan, China, 2014, paper FTh2F.2.
27. M. Laurila, M. M. Jørgensen, K. R. Hansen, T. T. Alkeskjold, J. Broeng, and J. Lægsgaard, "Distributed mode filtering rod fiber amplifier delivering 292 W with improved mode stability," Opt. Express **20**, 5742–5753 (2012).
28. C. Jauregui, H.-J. Otto, N. Modsching, O. de Vries, J. Limpert, and A. Tünnermann, "The impact of photodarkening on mode instabilities in high power fiber laser systems," presented at Advanced Solid State Lasers, Shanghai, China, 2014, paper ATh2A.1.
29. B. Samson, G. Frith, A. Carter, and K. Tankala, "High-power large-mode area optical fibers for fiber lasers and amplifiers," in *OFC/NFOEC* (2008).
30. M. N. Ozisik, *Heat Conduction*, 2nd ed. (Wiley, 1993).
31. I.-N. Hu, C. Zhu, C. Zhang, A. Thomas, and A. Galvanauskas, "Analytical time-dependent theory of thermally-induced modal instabilities in high power fiber amplifiers," Proc. SPIE **8601**, 860109 (2013).
32. M. M. Jørgensen, K. R. Hansen, M. Laurila, T. T. Alkeskjold, and J. Lægsgaard, "Modal instability of rod fiber amplifiers: a semi-analytic approach," Proc. SPIE **8601**, 860123 (2013).
33. M. M. Jørgensen, K. R. Hansen, M. Laurila, T. T. Alkeskjold, and J. Lægsgaard, "Fiber amplifiers under thermal loads leading to transverse mode instability," Proc. SPIE **8961**, 89612P (2014).
34. C. Spiegelberg, J. Geng, Y. Hu, Y. Kaneda, S. Jiang, and N. Peyghambarian, "Low-noise narrow-linewidth fiber laser at 1550 nm," J. Lightwave Technol. **22**, 57–62 (2004).
35. A. V. Smith and J. J. Smith, "Increasing mode instability thresholds of fiber amplifiers by gain saturation," Opt. Express **21**, 15168–15182 (2013).
36. J. P. Koplow, D. A. V. Kliner, and L. Goldberg, "Single mode operation of a coiled multi-mode fiber amplifier," Opt. Lett. **25**, 442–444 (2000).
37. K. Hejaz, A. Norouzey, R. Poozesh, A. Heidariazar, A. Roohforouz, R. Rezaei Nasirabad, N. Tabatabaei Jafari, A. Hamedani Golshan, A. Babazadeh, and M. Lafouti, "Controlling mode instability in a 500 W ytterbium-doped fiber laser," Laser Phys. **24**, 025102 (2014).
38. D. Marcuse, "Curvature loss formula for optical fibers," J. Opt. Soc. Am. **66**, 216–220 (1976).
39. R. Schermer and J. Cole, "Improved bend loss formula verified for optical fiber by simulation and experiment," IEEE J. Quantum Electron. **43**, 899–909 (2007).
40. M. L. Stock, C.-H. Liu, A. Kuznetsov, G. Tudury, A. Galvanauskas, and T. Sosnowski, "Polarized, 100 kW peak power, high brightness nanosecond lasers based on 3C optical fiber," Proc. SPIE **7914**, 79140U (2011).
41. T.-W. Wu, L. Dong, and H. Winful, "Bend performance of leakage channel fibers," Opt. Express **16**, 4278–4285 (2008).
42. L. Dong, K. Saitoh, F. Kong, P. Foy, T. Hawkins, D. Mcclane, and G. Gu, "All-solid photonic bandgap fibers for high power lasers (Invited Paper)," Proc. SPIE **8547**, 85470J (2012).